Computer Vision Based Measurement of Wildfire Smoke Dynamics

Marin BUGARIĆ, Toni JAKOVČEVIĆ, Darko STIPANIČEV
FESB, University of Split, 21000 Split, Croatia
toni.jakovcevic@fesb.hr

***Abstract*—This article presents a novel method for measurement of wildfire smoke dynamics based on computer vision and augmented reality techniques. The aspect of smoke dynamics is an important feature in video smoke detection that could distinguish smoke from visually similar phenomena. However, most of the existing smoke detection systems are not capable of measuring the real-world size of the detected smoke regions. Using computer vision and GIS-based augmented reality, we measure the real dimensions of smoke plumes, and observe the change in size over time. The measurements are performed on offline video data with known camera parameters and location. The observed data is analyzed in order to create a classifier that could be used to eliminate certain categories of false alarms induced by phenomena with different dynamics than smoke. We carried out an offline evaluation where we measured the improvement in the detection process achieved using the proposed smoke dynamics characteristics. The results show a significant increase in algorithm performance, especially in terms of reducing false alarms rate. From this it follows that the proposed method for measurement of smoke dynamics could be used to improve existing smoke detection algorithms, or taken into account when designing new ones.**

***Index Terms*—Image motion analysis, Computer vision, Computer aided analysis, Virtual reality, Pattern analysis.**

I. Introduction

Wildfires have always been devastating phenomena, having impact on natural and wildlife environment. Research shows [1] that wildfires destroy up to 10,000 km^2 of vegetation in Europe, and up to 100,000 km^2 in North America and Russia every year. In order to minimize the damage generated by wildfires, prompt reaction is essential. Traditional method for early discovery of wildfires is based on visual inspection of the surrounding terrain from lookout posts located on elevated areas. The primary phenomenon of interest is wildfire smoke rather than flame itself, since in most cases the smoke is visible before the flame. In majority of scenarios the fire is obscured and not remotely visible in its incipient phase, and becomes visible after it has considerably spread over larger areas.

Advances in technology have led to camera-based monitoring, where a single operator could simultaneously inspect multiple locations. One of the drawbacks of this approach is the decrease in human concentration over time, possibly leading to delayed detections. In recent times, progress in the field of computer vision has led to automatic smoke detection. Images acquired by the camera are analyzed by different computer algorithms raising the alarm in the case that smoke is present in the image.

There are many different approaches to visual smoke detection, however, there are several phases that are common to most smoke detection systems. One of the most common phases is the motion detection, where only the moving pixels are isolated and forwarded to subsequent detection phases [2-4]. Another important phase in the detection process is the chromatic analysis of the detected regions. Based on chromatic characteristics, certain categories of candidate regions can be rejected from the detection process [5,6]. Additional information about the candidate regions is obtained using texture analysis. There are diverse approaches to texture analysis in smoke detection, such as wavelet analysis [7] or the gray-level co-occurrence matrix (GLCM) [8]. Another phase that is common to most detection algorithms is the final or the decision phase. Utilizing the gathered information about the candidate regions, the system makes the final decision about raising the alarm. There are various approaches to the decision-making process such as neural networks [9], random forests [10] or support vector machines [11]. However, these systems are not completely autonomous, and require final confirmation from the operator.

Our motivation for this article is the analysis of smoke behavior, specifically smoke dynamics, in order to improve smoke detection systems. One of the drawbacks of most smoke detection algorithms is a high false alarm rate. There are different natural phenomena similar to smoke that could induce false alarms such as fog, clouds, dust etc. Nevertheless, smoke has specific dynamics that adhere to some general rules. In this article we analyze the specific information about these dynamic characteristics in order to create a classifier that could be used in smoke detection algorithms resulting in better discrimination between smoke and visually similar phenomena with different dynamics.

Several publications deal with dynamic characteristics of smoke, such as the ones described in [12-14] that use a simulation model of smoke spread. However, due to different location specific parameters that have to be set, these studies provide no adequate information that could be useful to improve smoke detection. For this reason, we have chosen an empirical approach to smoke dynamics analysis based on data collected from real wildfires.

Our intention is to measure the real dimensions of smoke plumes (in standard units of measurement), and to monitor the changes in size during the early stages of wildfire. In order to perform the measurements, we proposed a novel method to estimate those dimensions by using a video-based approach, or more precisely, by using GIS-based augmented reality (AR) and camera parameters. First, smoke plumes were recorded by the camera with known intrinsic and extrinsic parameters, as well as the exact geographic location. We hand-segmented smoke plumes from the

Digital Object Identifier 10.4316/AECE.2015.01008

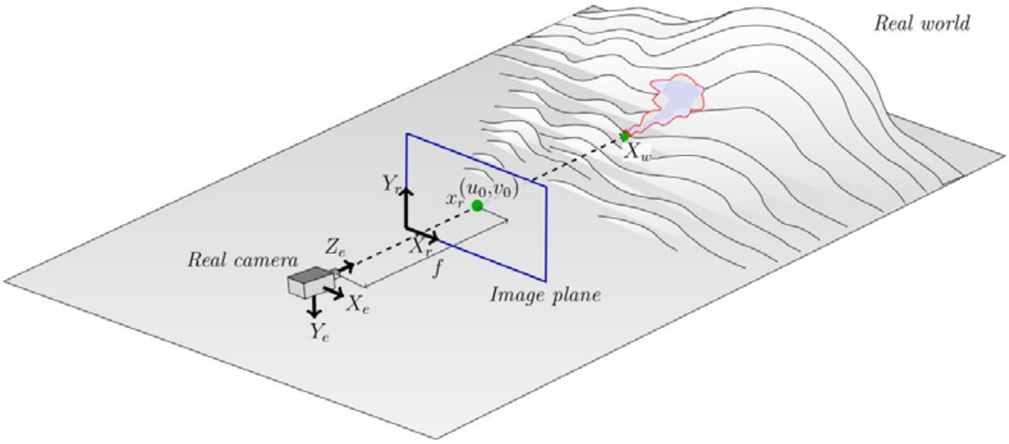

Figure 1. Image formation in the real camera model

training set images (in order to obtain maximum precision) and estimated their real dimensions by using the proposed method. We then analyzed smoke plume dynamics during the incipient phase of wildfire, since this phase is crucial for the early detection of smoke and exhibits different dynamics compared to a smoke of already expanded wildfires. Obtained smoke dynamics data served as training data for a classifier whose purpose is to distinguish smoke from phenomena with different dynamics. Finally, both the classifier and the proposed method were tested on a new set of video sequences containing both smoke and other phenomena that could induce false alarms.

II. Measurements of Smoke Dimensions

Smoke arising from wildfires moves in the open space, whereas its shape depends on the conditions prevailing in the surrounding environment. In the incipient phase of wildfire, it is possible to visually determine the smoke boundaries. However, determining the size of such phenomena, expressed in standard units of measurement (such as meters), might be a very difficult task.

In open space areas, even in ideal conditions, it is impossible to measure dimensions of smoke plumes directly on the spot. The smoke has a tendency of constant growth and ascent. Moreover, it is not always possible to approach the area affected by the wildfire. Therefore, in this paper we propose an alternative approach that could be used for the measurement of smoke dimensions. In our approach, we use CCD camera located at a safe distance from the wildfire.

Images taken by common CCD cameras do not contain the information about the third dimension. However, if camera's geographic location and parameters are known, GIS-based augmented reality could be used to estimate the physical size of the smoke visible in the image. The first step towards a successful measurement of smoke dimensions is to estimate the distance of the smoke visible in the image from the camera. Without this knowledge, the estimation is unreliable and prone to errors.

A. Distance Estimation Based on AR System

In order to compensate the lack of depth information of common CCD cameras, we propose the development of augmented reality system that incorporates the models of both real and virtual cameras, as well as the digital elevation of the surrounding terrain. This is important, since the topography of the terrain must be taken into account if one wants to estimate the distance from the camera to the specific point visible in the image. Augmented reality system provides the view of the physical, real-world environment with the additional computer generated information, in this case with the exact geographical coordinates of the specific points visible in the camera image. This information can then be used for the estimation of distances from the camera to these points.

The first step towards the development of such augmented reality system is generation of the appropriate digital terrain model. This virtual terrain model is based on the exact topography of the real world. Since we are dealing with wildfires that occur in the open space areas, it is possible to ignore artificial structures, such as the human infrastructures, that could affect the final appearance of the model. In order to preserve the dimensions of the real-world environment, a map projection must be chosen. Map projections define the systematic transformation of points on a sphere (or an ellipsoid) to points on a plane. We have chosen spherical map projection (EPSG code 3857) primarily because of its popularity and widespread usage.

The connection between the real-world terrain and the virtual terrain model is not sufficient for a successful augmented reality system, and therefore for a successful distance estimation. Each camera is different, and each camera view depends on specific set of parameters that define it. We use a pinhole camera model, defined by intrinsic and extrinsic camera parameters, as the representation of the real world camera. These parameters must be taken into account if the observed object is not perfectly positioned in the center of the camera image, which is almost always the case with wildfire smoke, since it moves unpredictably in the image.

Each virtual environment requires a virtual camera that defines what is visible in the virtual viewport. To create an augmented reality view with as few registration errors as possible, it is necessary to find a connection between the real and virtual camera models. Each point of the real-world environment visible in the real camera image must correspond to the point with the same geographic coordinates on the virtual terrain and must be visible at the same position in the virtual camera image.

Fig. 1 is a visual representation of image formation in the real camera model. The point in the real world X_W is visible in the camera image plane as the point x_r. In this example, it

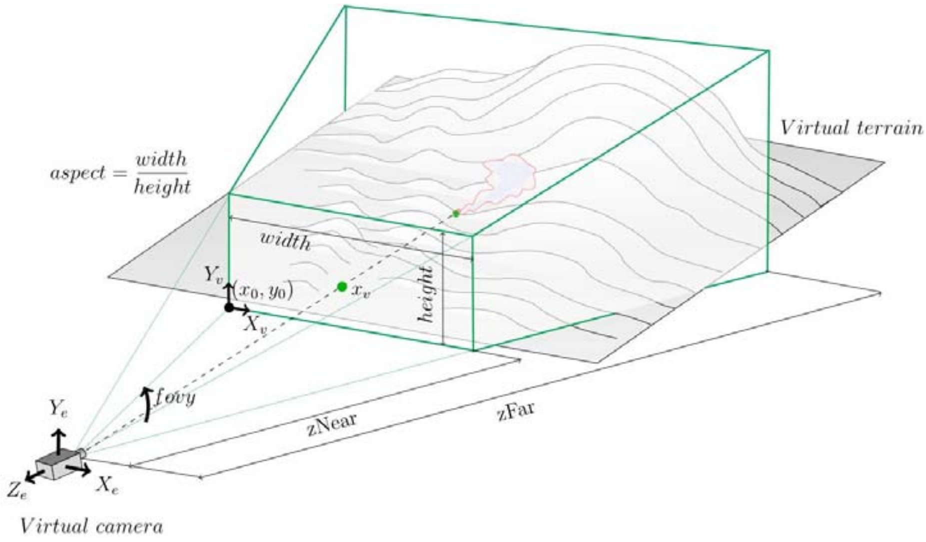

Figure 2. Image formation in the virtual camera model

is visible in the optical center, therefore point x_r has the coordinates (u_0,v_0). The focal length f is expressed in standard units of measurement, and should be converted to f_x, f_y expressed in pixels. Fig. 1 also displays orientation and position of camera coordinate system (X_e,Y_e,Z_e) and camera image coordinate system (X_r,Y_r).

If the point $x_r(X_r,Y_r)$ is not visible in the optical center, but in any other position in the image, its coordinates are calculated using the Eqs. (1)-(2).

$$X_r = f_x \frac{X_e}{Z_e} + u_0 \quad (1)$$

$$Y_r = f_y \frac{Y_e}{Z_e} + v_0 \quad (2)$$

Fig. 2 shows the simplified representation of the image formation for the virtual camera. Parameters used to define the view of the virtual (OpenGL) camera are the following: *height* and *width* of the image, (x_0,y_0) coordinates of the lower left viewport corner, *fovy* the field of view angle in radians in the y-direction and the *aspect* ratio that determines the field of view in the x-direction. Fig. 2 also shows the virtual camera coordinate system (X_e,Y_e,Z_e) and the virtual camera image coordinate system (X_v,Y_v). Part of the virtual terrain visible in the frustum defined by the distances *zNear* and *zFar* is rendered in the camera image. The equations used to calculate the coordinates of the point $x_v(X_v,Y_v)$ visible in the virtual viewport are the following:

$$X_v = \frac{\cot(fovy/2)}{aspect}\left(\frac{-X_e}{Z_e}\right)\frac{width}{2} + \frac{width}{2} + x_0 \quad (3)$$

$$Y_v = \cot(fovy/2)\left(\frac{-Y_e}{Z_e}\right)\frac{height}{2} + \frac{height}{2} + y_0 \quad (4)$$

After taking into consideration the differences in the orientation of the coordinate systems for both real and virtual cameras, it is possible to calculate the equations that define the connection between the image formation of the real and the virtual camera Eqs. (5)-(8).

The correct geographic location of the real camera is obtained using a GPS sensor. Since the virtual environment is correctly georeferenced, this information also represents the location of the virtual camera.

$$x_0 = u_0 - \frac{width}{2}, u_0 = x_0 + \frac{width}{2} \quad (5)$$

$$y_0 = \frac{height}{2} - v_0, v_0 = \frac{height}{2} - y_0 \quad (6)$$

$$fovy = 2\cot^{-1}\left(\frac{2f_y}{height}\right), f_y = \frac{height}{2\tan\left(\frac{fovy}{2}\right)} \quad (7)$$

$$aspect = \frac{width}{height}\frac{f_y}{f_x}, f_x = \frac{width}{height}\frac{f_y}{aspect} \quad (8)$$

If everything is correctly implemented into the augmented reality system, the virtual and real cameras share the same view, as seen in Fig. 3. More specifically, Eqs. (5)-(8) were implemented into the core of the Capaware [15,16] software that is an open source, 3D multilayer geographical framework developed as a virtual environment system with the ability to generate and display a virtual terrain. Apart from its functionality to serve as a visual analysis and decision-making system, Capaware has been used as a wildfire spread simulation [17] and a wildfire forecasting system [18]. None of the existing solutions and plugins for Capaware provided augmented reality functionality. In order to extend the system and convert it into an AR system, it was necessary to intervene into the core of the system. This intervention included abilities to display real camera image and to change virtual camera parameters defined by the Eqs. (5)-(8).

Smoke phenomenon covers a relatively large area in the surrounding environment; therefore it is necessary to choose a reference point on the terrain that will represent the position of the observed smoke. This point will be used for the actual estimation of the distance of the observed smoke from the camera. Smoke is constantly rising and it is not always linked to the ground, which further complicates the calculation of the distance to the observed phenomena. Determining the distance of the detected smoke plume is a difficult task not only for a computer system, but also for human operators [19]. Errors in determining the distance

Figure 3. An example of smoke plume from the real environment. Figure on the left represents a real camera view, whereas figure on the right represents the corresponding virtual camera view

of the smoke plume can occur either under the influence of the topographic shadowing [20] or incorrect identification of the base of the smoke. Therefore, one should be careful when determining the reference point that represents the position of the observed smoke region.

In our approach, the reference point should be as close to the smoke as possible and clamped to the ground in order to minimize the estimation error. We propose that this point is defined as the intersection of the virtual terrain and the ray cast from the camera which passes through the region of smoke. We have chosen the intersection of the ray with the virtual terrain located at a minimum distance from the camera as the reference point.

As already mentioned, smoke plumes are not always connected to the ground. Plume floating high in the air can in many times lead to the errors in distance estimation. Another unfavorable scenario occurs when a part of the observed smoke plume is obscured behind the elevated terrain. Nevertheless, the evaluation of the proposed smoke dynamic characteristics shows that, despite of these imperfections, it is still highly practical for the improvement of visual smoke detection systems. More details on this are given in Section 4.

Since camera's geographic coordinates are obtained using a GPS sensor, and coordinates of the reference point are known (each point on the virtual terrain is georeferenced), we can easily estimate the distance between the camera and the smoke plume.

B. Estimating the Smoke Region Size

Each pixel in the camera image represents a three dimensional space in the real world. The actual dimensions of this three dimensional space are not known, however, for a chosen reference point, it is possible to calculate the dimensions of the projection of the space surrounding this point onto the plane that has the following characteristics: it is located at the same distance from the camera as the reference point, and it is parallel to the camera image plane.

Fig. 4 demonstrates the method of dimensions estimation of the 3D space projected to the plane *R* that is parallel to the camera image plane and that holds the chosen reference point $T_{UTM}(X,Y,Z)$. Pixel $T_p(x,y)$, visible in the image plane at the position (x,y), represents a three dimensional space in the environment around the reference point $T_{UTM}(X,Y,Z)$ that is projected to the camera image plane.

Two points T_{UTM1} and T_{UTM2} located on the plane *R* are chosen in such a way that they are equidistant from the reference point for some distance d. Points T_{UTM}, T_{UTM1} and T_{UTM2} share a same Z coordinate, or in other words these points are located at the same altitude. Points T_{p1} and T_{p2} visible in the camera image plane are projections of points T_{UTM1} and T_{UTM2}, respectively. Points T_{p1}, T_p and T_{p2} lie on a same, horizontal line on the camera image plane. The length of the line segment $|T_{p1}\ T_{p2}|$ is denoted as $2d_p$.

For any chosen distance d, the distance d_p is unambiguously identified in the chosen virtual environment. Note that the distance d_p is expressed in number of pixels, and the distance d is expressed in meters. Since d_p and d represent the same distance, the connection between those two measurement units can be easily calculated. In case of square pixels this connection is the same in both horizontal and vertical direction. Otherwise, it is necessary to determine the connection between those measurement units in the vertical direction as well.

Note that after applying the Eqs. (5)-(8) the connection between the real and the virtual system has been found. Therefore the movement in any direction in the virtual environment represents the same movement in the real world. Also, sizes of the objects in the virtual environment correspond to the sizes of the objects in the real world.

Based on the proposed method, it is possible to estimate the total area covered within one pixel of the input image where the reference point is visible. Consequently, the area occupied by the smoke phenomena could also be projected to the previously specified plane. In order to simplify the estimation process, after estimating the surface area on the specified plane within the pixel where the reference point is visible and after counting the number of pixels where the smoke phenomenon is visible, it is possible to approximate the surface area of the projection of the smoke phenomena onto the plane R.

Since the distance of the smoke phenomenon from the camera is defined in meters (m), the calculated surface area is defined in square meters (m^2).

III. MEASUREMENT RESULTS AND ANALYSIS

In this section our aim is to define a logistic classifier capable of distinguishing smoke from visually similar phenomena with different dynamics based on one feature: the change in physical size. The measurement of physical size is based on methodology presented in Section 2. It is important to emphasize that this classifier is not intended to be used as a stand-alone classifier, but rather as a part of a smoke detection algorithm and used for elimination of

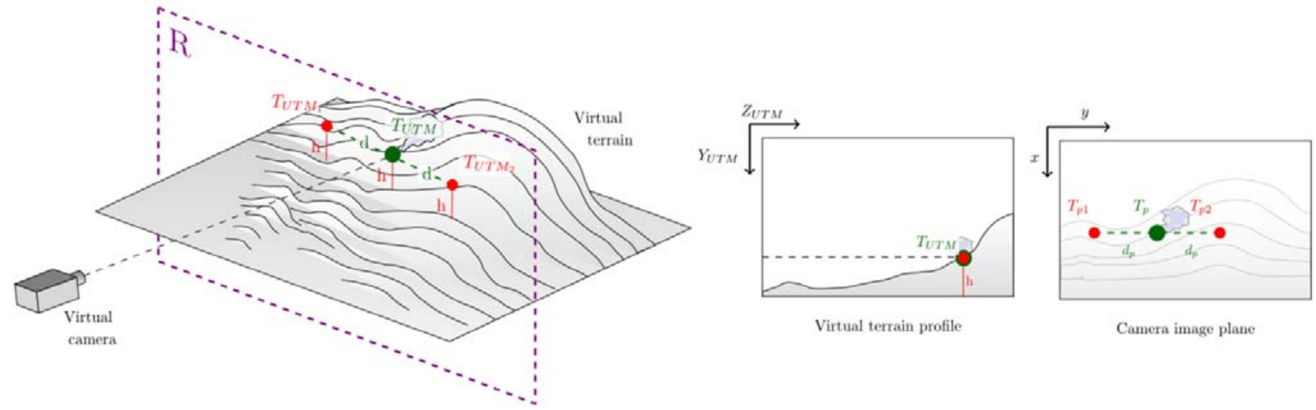

Figure 4. The procedure for estimating the size of the projection of 3D space that is visible within a single pixel on to the plane that contains the reference point T UTM and that is parallel to the camera image plane

certain categories of false alarms.

Training set for the classifier is obtained by performing the measurements of smoke dimensions followed by the analysis of smoke dynamics based on the obtained results. The measurements are conducted on offline smoke video database with known location information. The videos were recorded on various locations covering 33 different scenes containing smoke. Information about the geographical position of the camera is recorded for every scene along with specific intrinsic and extrinsic parameters. Development of smoke plumes in terms of size is tracked for the incipient phase of wildfire, since it is crucial for early detection. Each smoke plume is treated independently.

Total of 79 smoke plumes are tracked for a minimum period of 24 seconds up to 196 seconds depending on individual plume lifetime. To achieve maximum precision, tracking of separate smoke plumes is performed by hand-segmentation of input images in 4 second intervals. Using methods described in Section 2 we can estimate the physical smoke region size (in two-dimensional image plane) and analyze the change in this size over time. Obtained results are used to create a training set for our classifier. The average increase in smoke area in two-dimensional image plane (μ) is 16.04 m^2/s in the initial fire starting phase, with a standard deviation (σ) of 76.33m^2/s. Our aim is to define a range of smoke behavior that covers approximately 99% of smoke spreading scenarios included in the training set data. This range can then be used by the classifier as a model to eliminate those regions with different dynamics than smoke.

To achieve this, we first plot a histogram showing the distribution of smoke area change in m^2 for 1 second periods averaged from change in 4 second intervals, as shown in Fig. 5. Our intention is to find a probability density function (*pdf*) that best fits the training data set histogram. In our case it is the *pdf* of *t location-scale* distribution, defined as:

$$f(x) = \frac{\Gamma\left(\frac{\nu+1}{2}\right)}{\omega\sqrt{\nu\pi}\,\Gamma\left(\frac{\nu}{2}\right)}\left[\frac{\nu+\left(\frac{x-\lambda}{\pi}\right)^{2}}{\nu}\right]^{-\left(\frac{\nu+1}{2}\right)} \tag{9}$$

where Γ is the gamma function, λ is the location parameter, ω represents the scale parameter, and *v* is the shape parameter. Parameter values used for fitting are λ= 18.85, ω = 37.48 and *v* = 1.96. The fitted *pdf* function plotted over the data distribution is shown in Fig. 5. The area under the probability density function (in interval [-∞,∞]) represents 100% of smoke spreading scenarios. Our aim is to find a safe range of smoke dynamics that would eliminate certain categories of false alarms while still covering over 99% of smoke spreading scenarios. One way to determine the probability that a real-valued random variable (smoke plume dynamics in our case) will be found in the specified interval is to use a cumulative distribution function (*cdf*). *Cdf* for t location-scale distribution is defined as follows:

$$p(l) = F(l \mid \lambda,\omega,\nu) = \int_{-\infty}^{l} \frac{\Gamma\left(\frac{\nu+1}{2}\right)}{\omega\sqrt{\nu\pi}\,\Gamma\left(\frac{\nu}{2}\right)}\left[\frac{\nu+\left(\frac{x-\lambda}{\pi}\right)^{2}}{\nu}\right]^{-\left(\frac{\nu+1}{2}\right)} dx \tag{10}$$

where *p* denotes the probability that an observation from the t location-scale distribution, will fall in the interval [−∞,l). Fig. 6 shows the *cdf* for the chosen t location-scale distribution. Using the *cdf* we can calculate the probability of observation falling in limited intervals. It is now possible to show if a certain interval covers over 99% of smoke spreading scenarios. The probability of an observation falling in the interval (μ − 6σ,μ + 6σ) can be calculated as:

$$p(\mu + 6\sigma) - p(\mu + 6\sigma) = 0.9924 \tag{11}$$

where μ = 16.04 is the average value, and σ = 76.33 is the standard deviation of the measured samples. Therefore, we can say that the interval [−441.94 m^2/s, 474.02 m^2/s] covers 99.24% of smoke spreading scenarios. This interval indicates the allowed change in smoke area in one second intervals. As specified in the interval the change in the area could be positive or negative which would suggest that the smoke is growing or shrinking. This area is measured in the plane intersecting smoke and parallel to the image plane as described in Section 2.

We can now dismiss potential false alarms with a high degree of certainty in case the candidate region dynamics fall out of the defined range. Many smoke detection algorithms are very sensitive to intensity changes, shadowing by clouds and reflections that generate sudden detections of large regions which could be safely eliminated using this classifier. Nevertheless, the percent of success (99.24%) should be taken with caution as it defines the probability of an observation falling into this interval only in situations when the distance is perfectly estimated. Smoke is a phenomenon that is constantly rising and not always linked to the ground, or can be partly hidden by the foreground terrain. All this can lead to the false identification of the reference point representing the smoke phenomenon location, what inevitably leads to a false distance estimation, and consequently to the undesirable estimation of smoke dynamics and a missed detection. The image database used in the evaluation included different smoke sequences where we covered various scenarios that could induce such unwanted scenarios.

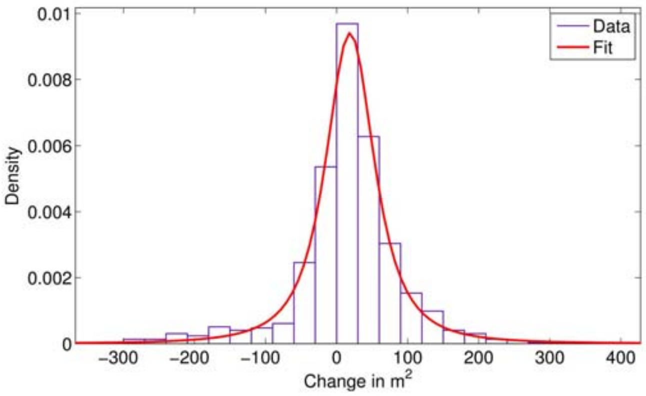

Figure 5. Distribution of the change in smoke area (m^2) for 1 second periods and the fitted function

IV. Evaluation

To demonstrate the applicability of the results presented in the previous section and to show how to use smoke dynamics characteristics to successfully improve standard smoke detection algorithms, we have performed a detailed evaluation using a database consisting of 10098 images. In this dataset, the smoke is present in 4474 of these images, whereas the remaining 5624 images include various other phenomena that are known to induce false alarms: such as clouds, shadowing by clouds, sea reflections, etc. We deliberately chose such demanding scenes (with a lot of movement present in the images) in order to show the full potential of the proposed smoke dynamics characteristics. Practice has shown that most false alarms occur during similar conditions, which justifies the use of such scenes for the evaluation. Representatives of the images used for the purpose of this evaluation are given in Fig. 7.

To perform the evaluation, we compared three different stages of smoke detection: motion detection, chromatic analysis (in combination with motion detection) and finally, smoke dynamics characteristics (also in combination with motion detection).

Motion detection is commonly used as the first step of the existing smoke detection algorithms, followed by additional phases of detection used for elimination of false alarms. The aim of this evaluation is to show how the proposed classifier based on smoke dynamics compares to standard chromatic analysis that is used as detection phase in the majority of state of the art smoke detection systems.

For motion detection we have chosen the approach proposed in [21]. The same motion detection algorithm has proven to be useful in smoke detection systems, as demonstrated in [22,23].

First step in this motion detection method is to build a statistical background model, that is:

$$class(I_n) = \begin{cases} |I_{n-1} - I_n| > \phi \cdot \overline{\sigma_n} & foreground \\ else & background \end{cases} \quad (12)$$

where I_n represents value of pixel I in the *n*th frame, ϕ is the

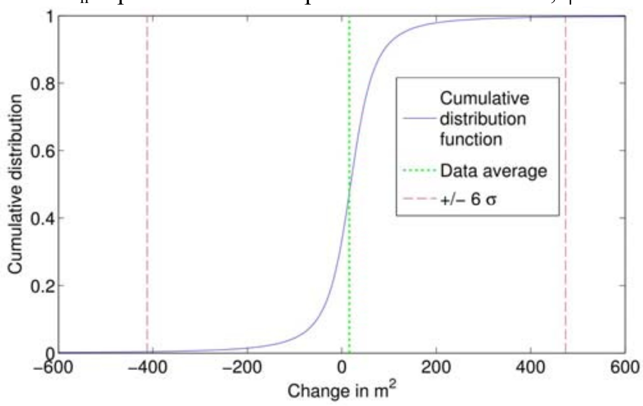

Figure 6. Cumulative distribution function (*cdf*) with marked data average and +/- 6 standard deviations of the measured samples

relative deviation threshold and $\overline{\sigma_n}$ represents standard deviation for a given pixel in the *n*th frame. Standard deviation is calculated as follows:

$$\overline{\sigma_{n+1}} = a\,|\,I_{n+1} - \overline{I_{n+1}}\,| + (1-a)\overline{\sigma_n} \quad (13)$$

where a is a parameter defining responsiveness of the model to the changes in the background, and $\overline{I_n}$ is the running average for a given pixel, calculated by

$$\overline{I_{n+1}} = a \cdot I_{n+1} + (1-a)\overline{I_n} \quad (14)$$

Parameters a and ϕ are variable parameters. In our case, we have chosen values a =0.08 and ϕ=1.7, although any other reasonable combination of parameters is also suitable.

For chromatic analysis phase we have chosen chromatic feature analysis model as described in [5]. It is based on the following three rules: i) the absolute difference of the maximum and minimum values among three components (RGB) should be less than a predetermined threshold , ii) the intensity I of a smoke pixel ranges between two given thresholds and iii) the value of B component is a slightly larger than two other components. The aforementioned rules were applied to the regions previously labeled as candidate regions by the same motion detection algorithm as before.

Finally, a third approach used for the evaluation is based on the same motion detection followed by the proposed method for measurement of wildfire smoke dynamics, where candidate regions were tested to verify that their dynamics fall into the interval [−441.94 m^2/s, 474.02 m^2/s], as proposed in the previous section.

Table 1 shows eight different quality measures [24] we use for the evaluation: measures for correct detections (*cd*), correct rejections (*cr*), false alarms (*fa*), missed detections (*md*), Matthews correlation coefficient (*mcc*), accuracy (*acc*), positive predictive value (*ppv*) and negative predictive value (*npv*). These measures are used to evaluate the performance of the algorithm with images as main evaluation units. The measures are defined as follows:

Figure 7. Representatives of the images used for the evaluation

TABLE I. EVALUATION RESULTS

	cd	cr	fa	md	mcc	acc	ppv	npv
Motion detection	0.9774	0.2304	0.4568	0.0226	0.2891	0.5340	0.4651	0.9371
Motion detection & chromatic feature analysis	0.9573	0.3793	0.3660	0.0427	0.3870	0.6164	0.5176	0.9274
Motion detection & smoke dynamics analysis	0.9192	0.6940	0.1773	0.0808	0.6104	0.7887	0.6856	0.9220

$$cd = \frac{TP}{TP + FN} \tag{15}$$

$$cr = \frac{TN}{TN + FP} \tag{16}$$

$$fa = \frac{FP}{TN + FP + TN + FN} \tag{17}$$

$$md = \frac{FN}{TP + FN} \tag{18}$$

$$mcc = \frac{TP \cdot TN - FP \cdot FN}{\sqrt{(TP + FP) \cdot (TP + FN) \cdot (TN + FP) \cdot (TN + FN)}} \tag{19}$$

$$acc = \frac{TP + TN}{TP + FN + FP + TN} \tag{20}$$

$$ppv = \frac{TP}{TP + FP} \tag{21}$$

$$npv = \frac{TN}{TN + FN} \tag{22}$$

where TP denotes the number of true positive detections, FN represents the number of false negative detections, TN represents the number of true negative detections, and FP represents the number of false positive detections.

Matthews correlation coefficient (*mcc*) is a balanced quality measure that works with classes of different sizes [25]. Accuracy (*acc*) is degree of closeness of measurements of a certain quantity to its actual value. Positive predictive value (*ppv*) and negative predictive value (*npv*) are the proportions of positive and negative results that are true positive and true negative results. For all these measures (*mcc*, *acc*, *ppv*, *npv*) value 1 represents best result.

The results from the evaluation based on the testing image set are presented in Table 1. The motion detection phase is generally used as a filter to reduce the amount of data to be analyzed, where only the detected regions are taken into account in following phases. The results show that the motion detection method successfully detects smoke, however, this phase alone cannot eliminate a significant amount of false alarms.

For the chromatic analysis phase following motion detection, the results show the performance of the detection has improved in terms of reduction in number of false alarms (*fa* measure reduces from 0.46 to 0.37) and an increase in the number of correct rejections (*cr* measure reduces from 0.23 to 0.38). Nevertheless, a small decrease in performance quality in the number of correct detections and missed detections is present as well.

In the approach based on motion detection followed by smoke dynamics analysis, we achieved a significant improvement in terms of reduction in the number of false alarms. More specifically, false alarms value (*fa)* has decreased from 0.46 to less than 0.18. Simultaneously, the number of correct detections (*cd)* remained higher than 0.90. Even more importantly, the value of correct rejections measure has increased to more than 0.69.

When observing other quality measures, the dynamic analysis approach shows same (*npv*) or better (*mcc*, *acc*, *ppv*) results when compared to chromatic analysis. This is especially evident for the *mcc* measure which is important in detection evaluation because it is a balanced measure which takes into account all detection cases (TP, TN, FP and FN). The results show a significant increase for the *mcc* measure when compared to chromatic analysis. More specifically, *mcc* measure for dynamic analysis has shown a significant increase to more than 0.60, what is significantly more than the increase to 0.38 shown for the chromatic analysis.

V. CONCLUSION

Wildfires are a constant threat to ecological systems, wildlife and human safety. Prompt reaction is one of the most important factors in minimizing the damages caused by wildfires. Since smoke is in most cases visible before the flame, wildfire detection methods are primarily focused on smoke detection. In order to provide a more effective means of smoke detection, automatic smoke detection systems have been developed, that can cover larger areas and serve as an aid for human observers. One of the main problems of these systems is the false alarms rate, where visually similar phenomena induce the system in triggering an alarm.

The main aim of this work is the measurement of real dimensions of smoke plumes in the incipient phase of wildfires and the analysis of dynamic smoke behavior in order to define the range of smoke region dynamics. This information could be used to improve the existing smoke detection methods in terms of eliminating potential false alarms based on dynamic behavior of the candidate regions.

Using an offline smoke video database with appropriate location information we measured the physical size of the smoke regions based on computer vision and augmented reality techniques. We have observed the change in size of the regions over time for 79 smoke plumes from various locations. The size change distribution can be fitted with a t location-scale distribution. Based on the cumulative distribution function it is possible to define the interval of smoke dynamics that covers over 99 percent of smoke region spreading scenarios. This interval is then used to create a classifier with a purpose to reliably reject phenomena visually similar to smoke, based on the dynamic behavior of the candidate regions.

Our aim was not to develop a new smoke detection algorithm, but to provide a classifier built on empirical data about smoke dynamics characteristics and a novel method for smoke dynamic measurements. These could be used to improve any existing smoke detection system by reducing the number of false alarms triggered by visually similar phenomena. Please note that the proposed classifier could be independently used in combination with any other method for measurement of wildfire smoke dynamics.

We performed a detailed evaluation where we demonstrated the possible improvement in performance of smoke detection algorithms. We compared evaluation results of the improvement based on smoke dynamics analysis with one variant of chromatic feature analysis phase, which is a standard phase in smoke detection. From these results it is evident that smoke dynamics is a very important feature in smoke detection that could distinguish smoke from visually similar phenomena. Therefore, it could be used to improve smoke detection quality, especially when there is a lot of movement present in the scene.

REFERENCES

[1] E. Kuhrt, J. Knollenberg, V. Mertens, "An automatic early warning system for forest fires", Annals of Burns and Fire Disasters, vol. 14, no. 3, pp. 151-155, 2001.

[2] B. U. Toreyin, Y. Dedeoglu, A. E. Cetin, "Contour based smoke detection in video using wavelets", in European Signal Processing Conference, EUSIPCO, Florence, 2006, pp. 1–5.

[3] P. Piccinini, S. Calderara, R. Cucchiara, "Reliable smoke detection in the domains of image energy and color", in IEEE International Conference on Image Processing, 2008, pp. 1376–1379. [Online]. Available: http://dx.doi.org/10.1109/icip.2008.4712020

[4] A. Genovese, R. D. Labati, V. Piuri, F. Scotti, "Wildfire smoke detection using computational intelligence techniques", in IEEE International Conference on Computational Intelligence for Measurement Systems and Applications (CIMSA), 2011, pp. 1–6. [Online]. Available: http://dx.doi.org/10.1109/cimsa.2011.6059930

[5] A. Ochoa-Brito, L. Millan-Garcia, G. Sanchez-Perez, K. Toscano-Medina, M. Nakano-Miyatake, "Improvement of a Video Smoke Detection Based on Accumulative Motion Orientation Model", in Electronics, Robotics and Automotive Mechanics Conference (CERMA) IEEE, 2011, pp. 126–130. [Online]. Available: http://dx.doi.org/10.1109/cerma.2011.27

[6] M. Anton, K. Olga, "Real-Time Smoke Detection in Video Sequences: Combined Approach, Lecture Notes in Computer Science", Springer Berlin Heidelberg, 2013, pp. 445–450. [Online]. Available: http://dx.doi.org/10.1007/978-3-642-45062-4_61

[7] W. Meng-Yu, H. Ning, L. Qin-Juan, "A Smoke Detection Algorithm Based on Discrete Wavelet Transform and Correlation Analysis", in International Conference on Multimedia Information Networking and Security (MINES), 2012, pp. 281–284. [Online]. Available: http://dx.doi.org/10.1109/mines.2012.46

[8] Y. Chunyu, Z. Yongming, F. Jun, W. Jinjun, "Texture Analysis of Smoke for Real-Time Fire Detection", in International Workshop on Computer Science and Engineering (WCSE), 2009, pp. 511–515. [Online]. Available: http://dx.doi.org/10.1109/wcse.2009.864

[9] Z. Xu, J. Xu, "Automatic Fire Smoke Detection Based on Image Visual Features", in International Conference on Computational Intelligence and Security Workshops, CISW, 2007, pp. 316–319. [Online]. Available: http://dx.doi.org/10.1109/cisw.2007.4425500

[10] J. Y. Kwak, B. C. Ko, J. Y. Nam, "Forest Smoke Detection Using CCD Camera and Spatial-temporal Variation of Smoke Visual Patterns", in International Conference on Computer Graphics, Imaging and Visualization (CGIV), 2011, pp. 141–144. [Online]. Available: http://dx.doi.org/10.1109/cgiv.2011.40

[11] J. Yang, F. Chen, W. Zhang, "Visual-Based Smoke Detection Using Support Vector Machine", in International Conference on Natural Computation, 2008. ICNC '08., 2008, pp. 301–305. [Online]. Available: http://dx.doi.org/10.1109/icnc.2008.219

[12] K. B. McGrattan, H. R. Baum, R. G. Rehm, "Numerical simulation of smoke plumes from large oil fires", Atmospheric Environment, vol. 30, no. 24, pp. 4125–4136, 1996. [Online]. Available: http://dx.doi.org/10.1016/1352-2310(96)00151-3

[13] W. Chow, R. Yin, "A new model on simulating smoke transport with computational fluid dynamics", Building and Environment, vol. 39, no. 6, pp. 611–620, 2004. [Online]. Available: http://dx.doi.org/10.1016/j.buildenv.2003.12.012

[14] H. M. Chang, A. F. Ghoniem, "A Computational Model for the Rise and Dispersion of Wind-blown, Buoyancy-driven Plumes. Part II.: Linearly Stratified Atmosphere", U.S. Department of Commerce, National Institute of Standards and Technology, MA, Cambridge, 1993. [Online]. Available: http://dx.doi.org/10.1016/1352-2310(94)90346-8

[15] M. Castrillon, P. A. Jorge, I. J. Lopez, A. Macıas, D. Martın, R. J. Nebot, et al., "Wildfire Prevention and Management in a 3D Virtual Environment", in GeoInformatics for Environmental Surveillance, statGIS09, Miloc, 2009.

[16] M. Castrillon, P. Jorge, I. Lopez, A. Macıas, D. Martın, R. Nebot, et al., "Forecasting and visualization of wildfires in a 3D geographical information system", Computers & Geosciences, vol. 37, no. 3, pp. 390–396, 2011. [Online] Available: http://dx.doi.org/10.1016/j.cageo.2010.04.011

[17] S. Yun, C. Chen, J. Li, L. Tang, "Wildfire spread simulation and visualization in virtual environments", in IEEE International Conference on Spatial Data Mining and Geographical Knowledge Services, ICSDM, Fuzhou, 2011, pp. 315–319. [Online]. Available: http://dx.doi.org/10.1109/icsdm.2011.5969054

[18] M. Castrillon, P. A. Jorge, A. Macıas, A. J. Sanchez, J. Sanchez, J. P. Suarez, et al., "Wildfire forecasting using an open source 3D multilayer geographical framework", in International Conference and Exhibition on Computer Graphics and Interactive Techniques, SIGGRAPH2009, New Orleans, 2009. [Online]. Available: http://dx.doi.org/10.1145/1597990.1598038

[19] S. Matthews, A. Sullivan, J. Gould, R. Hurley, P. Ellis, J. Larmour, "Evaluation of three fire detection systems", Bushfire Cooperative Research Centre, 2010.

[20] F. X. Catry, F. C. Rego, T. Santos, J. Almeida, P. Relvas, "Forest fires prevention in Portugal-Using GIS to help improving early fire detection effectiveness", in International Wildland Fire Conference, Seville, 2007.

[21] R. T. Collins, A. J. Lipton, T. Kanade, "A system for video surveillance and monitoring", in American Nuclear Society (ANS) Eight International Topical Meeting on Robotics and Remote Systems, Pittsburgh, Pennsylvania, 1999.

[22] T. Jakovčević, D. Stipaničev, D. Krstinić, "Visual spatial-context based wildfire smoke sensor", Machine vision and applications, vol. 24, no. 4, pp. 707–719, 2012. [Online]. Available: http://dx.doi.org/10.1007/s00138-012-0481-x

[23] M. Bugarić, T. Jakovčević, D. Stipaničev, "Adaptive estimation of visual smoke detection parameters based on spatial data and fire risk index", Computer Vision and Image Understanding, vol. 118, pp. 184–196., 2014. [Online]. Available: http://dx.doi.org/10.1016/j.cviu.2013.10.003

[24] T. Jakovčević, L. Bodrožić, D. Stipaničev, D. Krstinić, "Wildfire smoke-detection algorithms evaluation", in International Conference on Forest Fire Research, 2010, pp. 1-12.

[25] Matthews, B. W., "Comparison of the predicted and observed secondary structure of T4 phage lysozyme", Biochimica et Biophysica Acta, vol. 405, Issue 2, pp. 442-451, 1975. [Online]. Available: http://dx.doi.org/10.1016/0005-2795(75)90109-9